The Galaxy Population of Intermediate Redshift Clusters

Tomas Dahlén, Claes Fransson, Göran Östlin & Magnus Näslund
Stockholm Observatory, SE–106 91 Stockholm, Sweden

Abstract

Using photometric redshifts we discuss the galaxy population of the intermediate redshift clusters of galaxies Cl0016+16 at $z = 0.55$, Cl1600+41 at $z = 0.54$, Cl1601+42 at $z = 0.54$ and MS1008-1224 at $z = 0.31$. Comparing the clusters, we find no evidence for a universal shape of the total luminosity function (LF) at these redshifts. The LF of the early-type galaxies alone can, however, be described by a Gaussian, while the LF of the late-type galaxies is well fitted by a Schechter function. This suggests that the separate LFs for different populations may be universal. The difference in the total LFs can mainly be attributed to the varying relative normalisation of these populations, implying that clusters with an abundant population of late-type galaxies also have steeper faint-end slopes. In the cluster MS1008-1224 we detect a faint blue population that dominates over the population of red dwarf ellipticals, opposite to clusters at lower redshift.

Compared to low redshift clusters, we find that a general fading of the late-type population by $\sim$ 2 mag and the early-type population by $\sim$ 1 mag describes the evolution from $z = 0.55$ to $z = 0$ well. This evolution suggests that the total LFs of high-z clusters changes as the clusters get dynamically older, and therefore become more similar to local rich clusters.

As a consequence of the different early-type and late-type LFs and their dependence on cluster radius the fraction of blue cluster galaxies, as measured by the Butcher-Oemler effect, differs between the clusters and depends on limiting magnitude and radius.

We find a correlation between the dwarf-to-giant ratio and the surface density, indicating that the high density environment in the cluster cores is hostile to dwarf galaxies.

1 Introduction

Ever since the results of Butcher & Oemler (1984, hereafter BO84), showing that the fraction of blue galaxies in clusters increases rapidly between $z = 0$ and $z \sim 0.5$, it has been clear that there is strong evolution in cluster galaxy populations with redshift. These results have been confirmed by subsequent surveys (e.g. Rakos & Schombert 1995; Ellingson et al. 2001; Kodama & Bower 2001; Margoniner et al. 2001). A general picture explaining the over-all features of cluster formation and evolution is given within the hierarchical clustering scenario (e.g. Bower 1991; Kauffmann & White 1993; Kauffmann 1995; Baugh, Cole & Frenk 1996). A large number of observations and N-body simulations now support this scenario. The blueing with redshift of the cluster galaxies is explained by a higher accretion rate of star forming field galaxies at higher redshift (Bower 1991), possibly combined with a general increase in star formation in field galaxies at higher z (Diaferio et al. 2001). A consequence of the CDM model is that high-z clusters assemble during a much shorter time interval than comparably rich clusters today (Kauffmann 1995). This general scenario is also supported by the observed increase of mergers in high redshift clusters (van Dokkum et al. 1999). Furthermore, N-body simulations (e.g., Dubinski 1998) show that the brightest cluster galaxies (BCG) naturally form via mergers in a hierarchical scenario.

The difference in the radial distribution between early-type and late-type galaxies can be explained by the hierarchical model if infalling field galaxies, which are predominantly blue star forming galaxies, have their star formation truncated as they fall deeper into the cluster potential (Balogh, Navarro & Morris 2000; Diaferio et al. 2001). Mergers and interactions in the high density cluster environment also affect the star formation and can result in a transformation of galaxy morphology. This can explain the decreasing fraction of early-type galaxies found in clusters at higher redshift (van Dokkum et al. 2000).

One of the most important probes of cluster evolution is the luminosity function (hereafter LF), describing the number of galaxies per magnitude bin in a cluster. Binggeli, Sandage & Tammann (1988) showed that the total LF for the local Virgo cluster is a sum of several individual LFs, with different shapes for different galaxy types. At $M_B \lesssim -18$, ellipticals, as well as the different spiral types, have Gaussian LFs. At faint magnitudes, $M_B \gtrsim -18$, dwarf ellipticals (dEs) and irregulars dominate. This part of the LF is well represented by a Schechter function (Schechter 1976) with a steep faint-end slope. This results in a total LF that rises as a Gaussian at bright magnitudes and then flattens to a "plateau" (or even a slight decrease), before it turns steep at faint magnitudes. LFs with similar shapes are found in other nearby clusters, e.g. Coma (Trentham 1998a). The existence of a numerous population of faint dwarf galaxies in clusters, more common than in the field, is verified by a number of observations (e.g., Smith, Driver & Phillipps 1997; Wilson et al. 1997; Phillipps et al. 1998; Trentham 1998a; Yagi et al. 2002). There are, however, also clusters that do not show this steep increase at faint magnitudes (Trentham 1998b, 1998c). Most likely, this is a consequence of different evolution depending on e.g., richness and epoch of formation.

In a recent paper Conselice, Gallagher & Wyse (2001) discuss different scenarios that could lead to the dwarf population in local clusters. By comparing models with the observed kinematic and spatial properties of a number of Virgo cluster galaxies, they suggest that a transformation of spirals into dEs by "galaxy harassment" (Moore, Lake & Katz 1998) is occurring. Some dEs may, however, have formed outside the cluster in galaxy groups, which were later accreted. These dEs may therefore be as old as the cluster ellipticals. The fading of these cluster galaxies into todays dwarf population is discussed by Wilson et al. (1997) and Smail et al. (1998).

A consequence of the hierarchical scenario is that clusters observed at high redshift ($z \gtrsim 0.5$), were the spiral infall is assumed to peak (Bower, Kodama & Terlevich 1998), should have a higher fraction of spirals compared to local clusters. This should also lead to a differential evolution between the late-type and early-type LFs with redshift, with the late-type LF shifted towards brighter magnitudes at increasing redshift, as compared to the early-types.

Because it is observationally costly, if at all possible, to obtain redshifts for the numerous faint population, most observational efforts to study galaxy populations in high-z clusters have concentrated on the brighter galaxies ($M_B \lesssim -19$). Recently, however, photometric redshifts have been demonstrated to be a powerful tool for studying especially the faint population of cluster galaxies. Even though the accuracy of photometric redshifts can not be compared to spectroscopic redshifts, they can provide a reliable determination of clusters membership, and therefore significantly reduce the necessary amount of field galaxy subtraction. In a previous paper (Dahlén, Fransson & Näslund 2002, hereafter DFN02), we demonstrated the use of photometric redshifts in a study of the population of the intermediate rich cluster Cl1601+42 at $z = 0.54$.

The photometric redshift selection minimises the amount of background subtraction needed. Internal properties of the cluster, such as radial distribution and luminosity function, both for the total cluster population, as well as for different populations separately, can therefore be determined. Here we extend our previous study of Cl1601+42 to include two additional rich clusters, Cl0016+16 at $z = 0.55$ and MS1008-1224 at $z = 0.31$. We also include observations of a fourth poor cluster, Cl1600+41 at $z = 0.54$.

Throughout this paper we assume a Hubble constant $H_0 = 50$ km s^{-1} Mpc^{-1}, and a cosmology with $\Omega_M = 0.3$ and $\Omega_\Lambda = 0.7$, unless anything else is assumed. Magnitudes are given in the Vega based system.

2 The Data

2.1 Observations

The positions of the four clusters and a blank field, used for background subtraction, are listed in Table 1. All observations, except those of MS1008-1224, were carried out with the 2.56m Nordic Optical Telescope (NOT) and the Andalucia Faint Object Spectrograph and Camera (ALFOSC) during six observing runs between 1997 and 2001. The clusters and the background field were

Table 1: Positions of the observed clusters and back ground field given in J2000 coordinates.

Object	RA	Dec
Cl0016+16	$00^h18^m33^s.3$	$16^\circ\ 26'\ 36''$
Cl1600+41	$16^h02^m06^s.1$	$41^\circ\ 01'\ 23''$
Cl1601+42	$16^h03^m09^s.8$	$42^\circ\ 45'\ 18''$
MS1008-1224	$10^h10^m34^s.1$	$-12^\circ\ 39'\ 48''$
Blank field	$16^h08^m54^s.0$	$41^\circ\ 34'\ 00''$

Table 2: Log of observations.

Object	Filter	Obs. date	Exp. time	# of exp.	Seeing	1σ (mag arcsec^{-2})
Cl0016+16	B	Aug 00	18000s	20	$0''.92$	27.7
	V	Aug 00	17100s	19	$1''.03$	27.3
	R	Aug 00	7200s	8	$0''.73$	26.6
	I	Aug 00	16200s	36	$0''.74$	26.0
Cl1600+41	B	Jun 01	18000s	20	$0''.89$	27.8
	V	Jun 01	12600s	14	$0''.86$	27.2
	R	Jun 01	8100s	9	$0''.89$	26.7
	I	Jun 01	18000s	30	$0''.83$	26.2
Cl1601+42	U	Apr/Jun 99	25200s	14	$0''.89$	26.7
	B	Jun 98	12600s	14	$0''.84$	27.5
	V	Apr 99	16200s	18	$1''.02$	27.3
	R	Jun 97	7200s	8	$0''.75$	26.8
	I	Jun 98/Jun 99	14400s	24	$0''.76$	26.2
Blank field	B	Aug 00	16200s	18	$1''.15$	27.6
	V	Jun 99	16200s	18	$1''.02$	27.0
	R	Jun 97	7200s	8	$0''.70$	26.8
	I	Aug 00	16200s	36	$0''.73$	26.8

observed in four filters, B, V, R and I, and additional observations in the U filter were obtained for Cl1601+42. Observations were performed under photometric conditions. The seeing in the images varies between $0''.70$ and $1''.15$. A complete log of the observations is given in Table 2.

The observations of MS1008-1224 were carried out by the Science Verification Team at ESO using FORS at the VLT. The cluster was observed in B, V, R, I FORS Bessel filters with exposure times $\sim\ 1 - 1.5$h. The images were reduced using the IRAF package. The seeing in the final coadded frames is ($0''.72$, $0''.65$, $0''.64$, $0''.55$) in the (B, V, R, I) filter. Further details can be found at the ESO web site[1]. Information on redshifts, galactic extinction, observed area, X-ray luminosities and velocity dispersion of the clusters is given in Table 3.

2.2 Data reductions

The data obtained with the NOT were reduced using the IRAF package. Bias subtraction and flat-fielding were made in a standard manner. For the I–band we constructed a fringe-frame after removing objects from the science images. The fringe-frame was then subtracted from each science image, scaled to the appropriate background level. The images were corrected for atmospheric extinction, aligned, and finally combined. Calibration was done using standard stars from Landolt (1992). The galaxies were corrected for galactic extinction according to Schlegel, Finkbeiner & Davis (1998). A description of data reduction and calibration of the MS1008-1224 images are given at the ESO web page.

Photometry was obtained using the FOCAS package (Jarvis & Tyson 1981; Valdes 1982; Valdes 1993). The detection limit was set to 3σ of the sky noise, and a minimum detection area corresponding to the seeing-disk was used. For each object and filter we made a catalogue listing

[1] URL http://www.hq.eso.org/science/ut1sv

Table 3: Properties of the cluster sample.

Cluster	**Redshift**	A_V^a	**Observed area** sq. arcmin	**Diameter** Mpc	L_x (0.3-3.5 keV) 10^{44} erg s^{-1}	σ km s^{-1}
Cl0016+16	0.546[b]	0.19	32.5	3.1	34.7[c]	1703[c]
Cl1600+41	0.540[h]	0.04	28.9	2.9	<2.0[h,i]	-
Cl1601+42	0.539[d]	0.03	30.4	3.0	2.1[c]	1166[c]
MS1008-1224	0.306[e]	0.23	32.4	2.2	5.8[f]	1054[g]

Notes:
a) Schlegel et al. 1998
b) Dressler & Gunn 1992
c) Smail et al. 1997.
d) Oke, Gunn & Hoessel 1996.
e) Lewis et al. 1999.
f) Gioia & Luppino 1994.
g) Carlberg et al. 1996.
h) Henry et al. 1982.
i) Converted from energy band 0.5-4.5 keV assuming electron temperature 4 keV

Table 4: Number of objects with $m_R < 25$ in the different images, and the number of objects with aperture photometry in four to five filters, three filters, and one or two filters only. Stars are excluded.

Image	**No. of Objects**	**$\geq$ 4 filters**	**3 filters**	**1-2 filters**
Cl0016+16	1430	1154	172	104
Cl1600+41	809	791	13	5
Cl1601+42	1199	1034	106	59
MS1008-1224	1665	1544	104	17
Field1	945	781	87	77

isophotal magnitude, aperture magnitude, position and area. When calculating the aperture magnitude we first smoothed the observations to the seeing of the filter with the worst seeing of each cluster, and then used a constant aperture size with a radius corresponding to this seeing. Finally, a combined catalogue for each object was made by using the positions in the R–catalogue and matching these with the positions in the other catalogues.

The completeness was tested with simulations where we added artificial galaxies with different magnitudes and radial profiles to the real images. Using the same detection procedures as for the real data we find that 100 per cent of the galaxies are detected down to $m_R = 25$ for all our objects. Using simulations we also calculate corrections that should be applied when calculating total magnitudes from the observed isophotal magnitudes. These simulations are described in Näslund, Fransson & Huldtgren (2000) and DFN02.

In Table 4 we list the number of objects in each catalogue to a limiting magnitude $m_R < 25$. We also list the number of objects having aperture photometry in at least four filters (i.e four or five filters for Cl1601+42, and four filters for the other object), three filters, as well as in two or one filter only. Objects identified as stars by visual inspection of the psf, are excluded.

3 Photometric redshifts

An extended discussion on the use of photometric redshifts applied to clusters of galaxies is given in DFN02. Here we present a brief summary of the technique. For every object we minimise the expression

$$\chi^2(t, z, m_\alpha) = \sum_i \frac{(m_i - (T_i(t, z) + m_\alpha))^2}{\sigma_i^2} \quad (1)$$

where m_i and σ_i are the observed magnitudes and uncertainties in filter i, respectively. $T_i(t,z)$ is the magnitude in the i–filter of template t, redshifted to z. This magnitude is calculated by convolving the filter curve and the quantum efficiency of the detector with the galaxy template. The quantity m_α is a constant, which fits the apparent magnitude of the template galaxy.

A set of ten different templates are used. We construct these by interpolations between the four observed galaxy templates given by Coleman, Wu & Weedman (1980). These represent E, Sbc, Scd and Im galaxies. Absorption due to intergalactic H I clouds is treated as in Madau (1995). We also include eight stellar templates of M–dwarfs taken from Gunn & Stryker (1983). For a discussion of possible systematic effects when using photometric redshifts see DFN02.

A modification compared to DFN02 is that we here use a "Bayesian" approach (e.g. Kodama, Bell & Bower 1999; Benitez 2000). This method allows the incorporation of pre-existing knowledge about the galaxies into the photometric redshift determination. This is illustrated in Figure 1, where we in the top panel show the probability distribution derived from the chi-square fit according to Eq.(1), for a galaxy with known spectroscopic redshift $z = 0.31$. There are ten local minima in the chi-square fit, resulting in ten probability maxima, divided into two groups, one at low, and one at high redshifts. The best-fitting template is in this case an Sa galaxy with redshift $z = 0.20$, but almost as good fits are achieved for the three other templates with $z < 0.5$, representing E to Sbc galaxies. There are also maxima with high probability at $z \sim 2.8 - 3.5$. The degeneracy of the high and a low redshift groups arise because the Lyman-break falls approximately between the same filters at $z \sim 3.5$, as the 4000 Å break does at $z \sim 0.3$.

The absolute magnitude for this galaxy at $z \sim 3.5$ would, however, be unrealistic, $M_B \sim -28$, whereas at $z \sim 0.1$ and $z \sim 0.3$ we get $M_B \sim -18$ and $M_B \sim -20.5$, respectively. To account for this one could weight the probability function with an expected LF, an approach used by Kodama et al. (1999). However, since we are here interested in *determining* the LF, we can not use this method. Instead, we use an exponential cut-off two magnitudes brighter than M_B^*, where M_B^* is determined by a fit to the Schechter function without any weighting. The effect of introducing this cut-off at bright magnitudes is mainly to suppress the false peaks introduced by the misidentification between the Lyman–break and the 4000 Å break. An alternative would be to truncate the procedure at e.g. $z = 2$. However, at $m_R \sim 25$, galaxies at $z \gtrsim 2$ with "normal" absolute magnitudes are expected; a cut-off could here lead to a misidentification of these galaxies. Furthermore, the volume element increases with redshift (up to $z \sim 1.8$, dotted line in the top panel of Figure 1). Therefore, of two maxima with the same probability from the chi-square fit, the higher redshift should for constant comoving density, be more likely due to the larger volume.

The lower panel of Figure 1 shows the probability distribution for the same galaxy after multiplying the result from the top panel with the probability distribution derived after applying an exponential cut-off at bright magnitudes and a weighting by the volume element. The distributions are normalised to unit area.

The peaks at $z > 2.5$ have now disappeared, and the lowest redshift peaks are suppressed due to the smaller volume element. The maximum probability is now for a Sb galaxy at $z = 0.31$, which matches the spectroscopic redshift.

The "Bayesian" approach we use mostly affects the determination of redshifts for the cluster MS1008-1224 at $z = 0.31$. Liu & Green (1998) show that when using photometric redshifts there is a risk of misidentification between Sbc galaxies at $z \sim 0.05$ and Scd/Im galaxies at $z \sim 0.3$. From our example above we also note that $\sim$ Sb galaxies at $z \sim 0.3$ can be misidentified as E galaxies at $z \lesssim 0.1$.

When estimating the dispersion between spectroscopic and photometric redshifts for 61 galaxies in the field of MS1008-1224, we find $\sigma_z \sim 0.051$, when we use the "Bayesian" approach, compared to $\sigma_z \sim 0.11$ without it. The increased dispersion is mainly due to a few galaxies achieving large errors. Excluding six galaxies reduces the dispersion to $\sigma_z \sim 0.058$. For the clusters at $z \sim 0.55$ the effect of including this weighting is marginal. Here we get $\sigma_z \sim 0.054$ with the "Bayesian" approach and $\sigma_z \sim 0.060$ without, when calculating the dispersion between the photometric and spectroscopic redshifts for 38 galaxies in the field containing Cl0016+16.

The example shown in Figure 1 was picked to illustrate the "Bayesian" method, and has an unusual high number of probability peaks with similar strengths. Most galaxies have a more

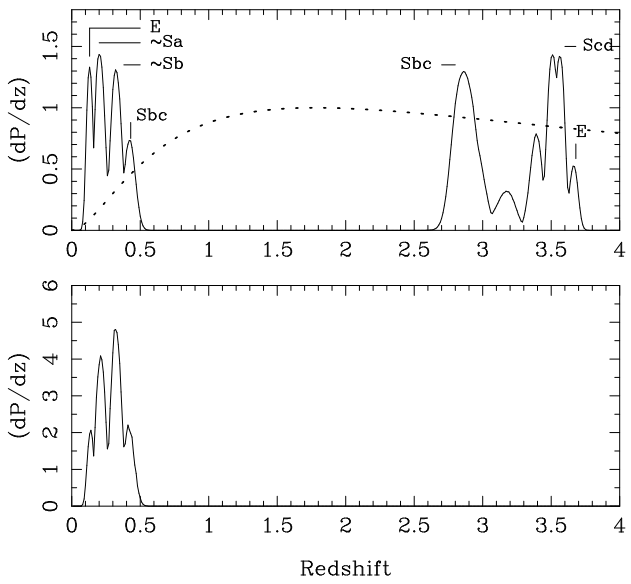

Figure 1: Chi-square probability function for the template fitting method, for a galaxy with known spectroscopic redshift $z = 0.31$. At each redshift the probability of the galaxy template that has the minimum chi-square, i.e the highest probability is plotted. The top panel shows the probability function without considering absolute magnitudes or volume element. The dotted line shows the redshift dependence of the volume element. In the bottom panel we use a cut-off at bright magnitudes, and take the volume element into account. For some of the peaks we plot the associated galaxy type. The distributions are normalised to unit area.

clearly defined primary peak.

3.1 Photometric redshift catalogue

We calculate photometric redshifts for all objects with $m_R \leq 25$ and aperture photometry in at least three filters, which corresponds to 92–99 per cent of the total number of objects to this limit (Table 4). The accuracy of the photometric redshifts is estimated by comparing our result with available spectroscopic redshifts. In Table 5 we list the number of available redshifts and the rms deviation between the photometric and spectroscopic redshifts, σ_z. The galaxies used for calculating the rms have photometry in all filters. To estimate the increase in errors for objects only having photometry in three filters, we also calculate the rms deviation after excluding the filter with the largest error for each galaxy, $\sigma_z^{(3)}$.

3.2 Comment on background counts

To estimate the background contamination we use $BVRI$ photometry of our blank field. In DFN02 we used $UBVRI$ photometry of the ESO Imaging Survey (EIS) deep field published by da Costa et al. (1998). Number counts to $R = 25$ for Field1 and the EIS field yield 983 $\pm$ 133 and 845 $\pm$ 120, respectively, where the fields are normalised to the same size as the image of Cl0016+16. Errors represent 1σ and include Poisson statistics and field-to-field variance (see DFN02 for a discussion). The resulting counts are therefore consistent within the errors.

When determining the background counts within the cluster redshift range, we find a larger deviation between the two fields. In the redshift range $z_{Cl0016} \pm 1.5\sigma_z$, we find 121 $\pm$ 20 galaxies for Field1, and 166 $\pm$ 26 galaxies for the EIS field to $R = 25$. These results are marginally within errors, but it is likely that there are systematic effects responsible for some of the off-set. In particular, the aperture magnitudes are determined differently. For our blank field we smooth the

Table 5: N is the Number of galaxies with spectroscopic redshifts used to determine the dispersion between photometric and spectroscopic redshifts, σ_z is the dispersion using information from all filters, while $\sigma_z^{(3)}$ is the dispersion using only three filters. Also given is the resulting number of clusters galaxies within $z_{Cl} \pm 1.5\sigma_z$ for the total areas and inside a common radius of 1 Mpc. We also list the density of background galaxies within each redshift range. The limiting magnitude is $M_B = -17.7$, corresponding to $m_R \sim 25$ at $z = 0.54$ and $m_R \sim 23.4$ at $z = 0.31$.

Cluster	z_{Cl}	N	σ_z	$\sigma_z^{(3)}$	Cluster galaxies		Background[a]
					Total area	$R < 1$ Mpc	(Mpc^{-2})
Cl0016+16	0.546	38[b]	0.054	0.080[c]	463 ± 32	248 ± 19	12.7±2.1
Cl1600+41	0.540	[d]	0.065[d]	0.10[d]	36 ± 24	26 ± 12	14.6±2.4
Cl1601+42	0.539	78[b]	0.076	0.12[e]	332 ± 35	154 ± 18	18.8±2.9
MS1008-1224	0.306	61[f]	0.051	0.067	221 ± 20	173 ± 16	11.6±2.3
MS1008-1224[g]					319 ± 26	240 ± 21	20.6±3.5

Notes:
a) Measured within the redshift range defining the different clusters, i.e. $z_{Cl} \pm 1.5\sigma_z$.
b) Dressler et al. 1999.
c) Excluding two outliers with large errors.
d) No spectroscopic redshifts available, except for central galaxy. We assume dispersions equal to the mean of the dispersions of the two clusters at similar redshift.
e) Excluding five outliers.
f) Yee et al. 1998.
g) Number of galaxies to $M_B = -16.2$.

images to the same seeing before calculating the colours, whereas the aperture magnitudes given for the EIS field have a varying seeing in the different bands. This can affect the colours, especially for small objects that do not cover the whole aperture.

To check the effect of this, we calculate photometric redshifts for the field containing Cl0016+16 without smoothing the images to the same seeing. Comparing with the 38 objects that have spectroscopic redshifts we find an rms deviation $\sigma_z = 0.078$, which is considerably larger than what we found after smoothing, $\sigma_z = 0.054$. Therefore, the photometric redshifts calculated for the EIS catalogue are likely to be less accurate.

Finally, systematic errors could be introduced by the uncertainty in the zero-point magnitudes and the use of different software when doing the photometry, i.e the use of FOCAS for Field1, and SExtractor for the EIS field.

To minimise the risk of introducing systematic errors, we use the photometry from our blank field in this analysis, since this is derived in the same way as the photometry of the cluster images. The use of a different background field does, however, not affect the result in DFN02 on Cl1601+42 more than marginally, i.e. any differences are within the quoted errors. This illustrates the advantage of the photometric method for examining high-z clusters; the relatively small corrections for background contamination makes the results less dependent on the background.

3.3 Cluster membership and galaxy classification

For selecting cluster members we use a redshift range $\pm 1.5\sigma_z$ around the mean redshift of the cluster, with values of σ_z given in Table 5. To account for the increase in dispersion for the galaxies only detected in three filters (Table 3), we use the corresponding $\sigma_z^{(3)}$ for these galaxies. Assuming that the errors are Gaussian, the $1.5\sigma_z$ cut should include ~ 86 per cent of the actual number of cluster galaxies to our limit. Taking into account the small fraction of the galaxies observed in three filters only that may result in outliers with large errors, we estimate that we include $\sim 80 - 85$ per cent of the total number of cluster galaxies when applying the 1.5σ cut. For a discussion on completeness and contamination when selecting cluster members using photometric redshift, see Brunner & Lubin (2000).

In this study we divide the galaxies into late-types and early-types, based on the spectral type determined by the photometric colours of the galaxies. The division is made half way between

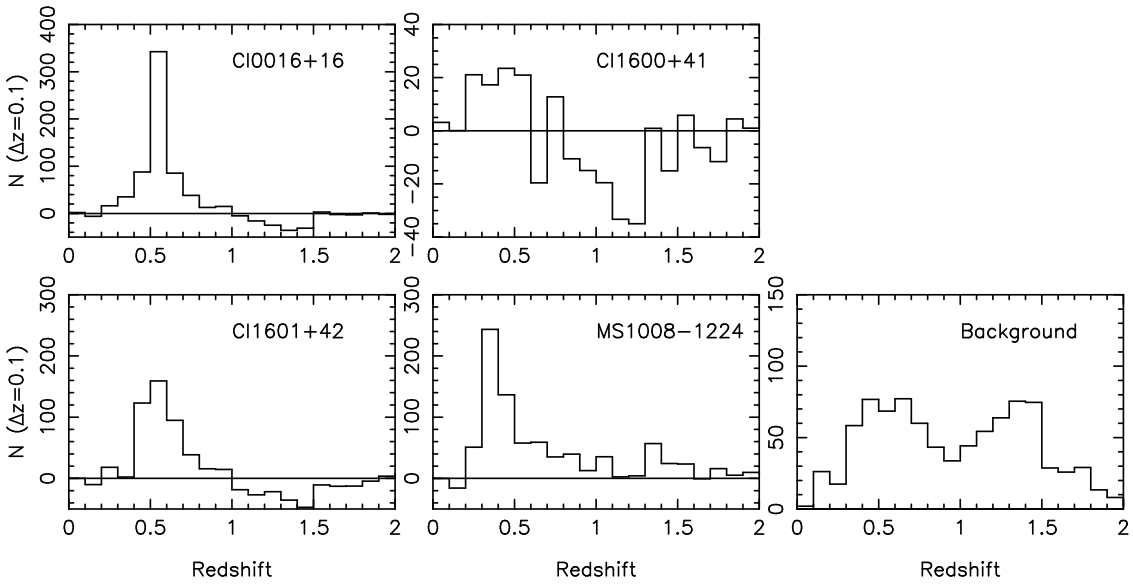

Figure 2: The left and the middle panels show the distribution of photometric redshifts in the cluster images after subtracting background galaxies. The right panel shows the redshift distribution of the background field. Note the different scales on the y-axis. The peak in the background distribution at $z \sim 1.4$ is most likely caused by the lack of IR photometry. All distributions above $z \sim 1$ should therefore be viewed by caution.

the E and Sbc templates from Coleman et al. (1980), approximately corresponding to a rest-frame colour $B - V = 0.8$. The first category consists of early-type galaxies with red colours, which are mostly ellipticals and lenticulars, but also include passive spirals with red colours. The second category includes late-type spirals and irregulars, with a possible inclusion of blue elliptical systems.

4 Results

The distribution of photometric redshifts in the cluster fields, after subtracting background galaxies, is shown in the left and middle panels in Figure 2. The right panel shows the redshift distribution of the background field. The location of the clusters is apparent for all clusters except Cl1600+41. We comment on this cluster in next subsection.

As a measure of the richness of the clusters we give in Table 5 the number of cluster galaxies with $M_B < -17.7$ for the total areas (see Table 3), as well as inside a common radius of 1 Mpc. We also list the density of background galaxies within the redshift range adopted for the different clusters. For the low redshift cluster, MS1008-1224, we also give numbers for $M_B < -16.2$.

In the left panel of Figure 3 we show the surface density of galaxies with $M_B < -17.7$ for the four clusters as a function of radius. The horizontal solid line marks the surface density of the background field in the redshift range of Cl1600+41. Error bars and dashed lines represent 1σ errors. The right panel of Figure 3 shows the projected fraction of early-type galaxies for the four clusters. The horizontal line marks the early-type fraction of the background field at $z \sim 0.55$, which is also similar to what we find at $z \sim 0.31$. All clusters have an early-type fraction clearly above the field value in the core region. In Cl0016+16 this fraction is ∼85 per cent in the core. This decreases with radius, but stays above 50 per cent for the whole area covered. The early-type fractions in Cl1601+42 and MS1008-1224 is ∼60 per cent in the core, and show a decrease which approaches the field value at large radius, even though the deviation from the field is still significant at the outermost points. For Cl1600+41, only the innermost point has a

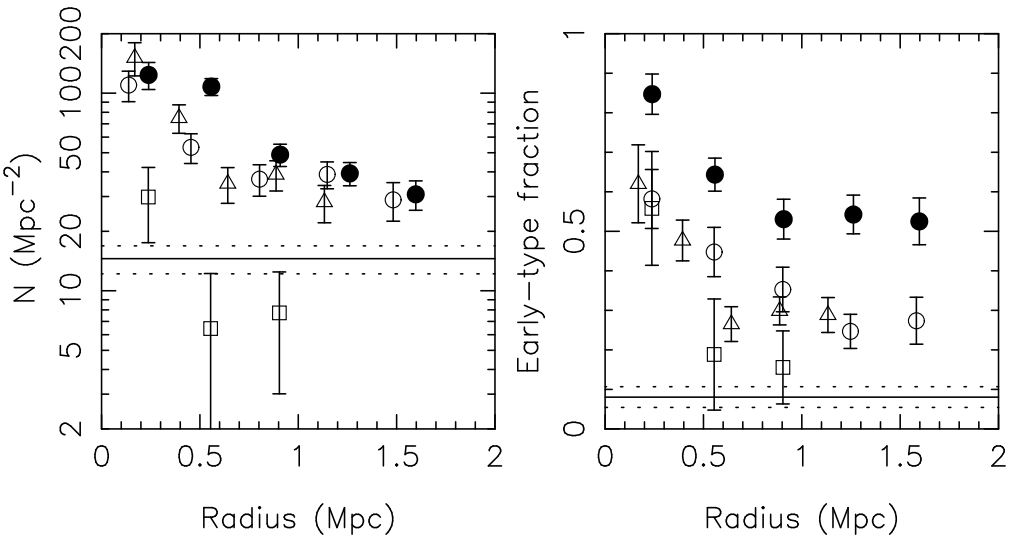

Figure 3: Left panel: Projected surface density as function of radius for Cl0016+16 (filled circles), Cl1600+41 (squares), Cl1601+42 (open circles) and MS1008-1224 (triangles). The horizontal line shows the surface density of the background field in the redshift range of Cl1600+41. Right panel: Early-type fraction as function of radius for the four clusters. The horizontal line shows the early-type fraction of the field at $z = 0.54$. The limiting magnitude is $M_B = -17.7$. Error bars and the dashed lines represent 1σ errors.

late type fraction deviating from the field. From both figures it is clear that we do not reach the field in any of the clusters, except Cl1600+41.

4.1 The poor cluster Cl1600+41

From the results above it is clear that Cl1600+41 is very poor, with only 36 ± 24 cluster galaxies with $m_R < 25$. Figure 3 also indicates that if at all significant, the radial extent of the cluster is less than ~ 0.5 Mpc. At larger radii the surface density is marginally below the field value, while the late type fraction is consistent with the late type fraction of the field.

The most significant indication of a cluster comes from the colour distribution, where the innermost point shows a clear excess of red galaxies (Figure 3). Also, the magnitude and colour of the central galaxy is similar to the brightest cluster galaxy (BCG) in the other clusters. Furthermore, a visual inspection of a three colour image of Cl1600+41 shows this bright red central galaxy to be surrounded by a number of red and blue galaxies, clearly indicating the presence of a cluster.

If we calculate the number of cluster galaxies in Cl1600+41 by the standard method of subtracting galaxies in a blank field from the cluster image in a *single* band, we get a total of 9 ± 127 cluster galaxies to $m_R < 25$. The large error is due to field-to-field variations, which dominate in the subtraction method. It is clear that the subtraction method would not result in any cluster detection when using our blank field as a reference for the background counts.

With only 36 selected cluster members within the chosen redshift range, the background counts dominate over the cluster galaxies, i.e. only 22 per cent of the galaxies are expected to be cluster galaxies, as compared to 78, 66 and 80 per cent, for Cl0016+16, Cl1601+42 and MS1008-1224. It is clear that this cluster is close to the detection limit. The large contamination in Cl1600+41 makes it impossible to determine either the internal properties of the cluster with any significance, or the cluster LF. Therefore, we do not include Cl1600+41 when comparing the LF and the BO effect between the clusters.

Table 6: Characteristic magnitude, M_B^* and faint-end slope, α derived from the Schechter function fit to the rest-frame B-band LFs for the total population and for late-type galaxies only. α_f is the slope of a straight line fit to the five faintest magnitude bins in each cluster. Limiting magnitude is $M_B = -17.7$. For MS1008-1224, we also give results to $M_B = -16.2$.

Cluster	**All galaxies**			**Late-types**		
	M_B^*	α	α_f	M_B^*	α	α_f
Cl0016+16	-21.07 ±0.24	-0.55 ±0.10	-0.65 ±0.10	-21.75 ±0.50	-1.12 ±0.17	-1.17 ±0.18
Cl1601+42	-21.87 ±0.36	-1.25 ±0.10	-1.33 ±0.14	-21.80 ±0.53	-1.53 ±0.27	-1.65 ±0.19
MS1008-1224	-21.06 ±0.17	-0.72 ±0.26	-0.99 ±0.15	-21.05 ±0.58	-1.11 ±0.33	-1.61 ±0.24
MS1008-1224[a]	-21.48 ±0.17	-1.46 ±0.09	-1.92 ±0.13	-22.00 ±0.37	-1.50 ±0.17	-1.89 ±0.16

Note:
a) Limiting magnitude $M_B = -16.2$.

Table 7: M_B^G is the peak magnitude and σ^G is the width of a Gaussian fit to to the rest-frame B-band LF for the early-type population brighter than $M_B = -18.0$.

Cluster	**Early-types**	
	M_B^G	σ^G
Cl0016+16	-20.27 ±0.08	1.01 ±0.05
Cl1601+42	-20.05 ±0.17	1.30 ± 0.10
MS1008-1224	-20.46 ±0.10	0.73 ± 0.06

4.2 The cluster luminosity functions

When calculating the LF we divide the galaxies within the cluster redshift range into magnitude bins with $\Delta m = 0.5$ to $M_B = -17.7$ for the two clusters at $z \sim 0.55$, and to $M_B = -16.2$ for MS1008-1224 at $z \sim 0.31$. K-corrections are determined for each galaxy using the best-fitting template from the photometric redshift calculations. For each magnitude bin we subtract background galaxies within the redshift range of the different clusters.

The left panels in Figure 4 show the resulting LFs for the three clusters. As a first step we fit the total LFs to the usual Schechter function (Schechter 1976),

$$\Phi(M) \propto e^{-10^{0.4(M^*-M)}} 10^{-0.4(\alpha+1)M}, \tag{2}$$

where M^* is the characteristic magnitude, representing the turnoff at the bright end of the LF profile, and α is the slope at the faint end of the LF. As an alternative to α, we also calculate the slope of a straight line fit to the five faintest bins in each LF, according to

$$\Phi_f(M) \propto 10^{-0.4(\alpha_f+1)M}. \tag{3}$$

(Trentham 1998a; DFN02). The parameter α_f gives a better representation of the faint-end of the LF, since it is not affected by the coupling between M^* and α in the Schechter function. In Table 6 we list M^*, α and α_f for the clusters. Parameters are given both for the total cluster populations, and for the late-type population in each cluster.

Figure 4 shows that the shapes of the LFs of the three clusters differ substantially. To further understand these differences, we plot the LFs divided into early-type and late-type galaxies separately in the right panels of Figure 4. For all three clusters, the early-type galaxies with $M_B \lesssim -18$ have a Gaussian LF, peaking at $M_B^G \sim -20$ (Table 7). We note that the faint early-type population in MS1008-1224 shows an increase below $M_B = -18$. We return to this point in Section 5.

The late-type galaxies are better fitted by Schechter functions. However, the relative normalisations of the early-type and late-type LFs vary between the different clusters. In Section 5 we discuss these differences further.

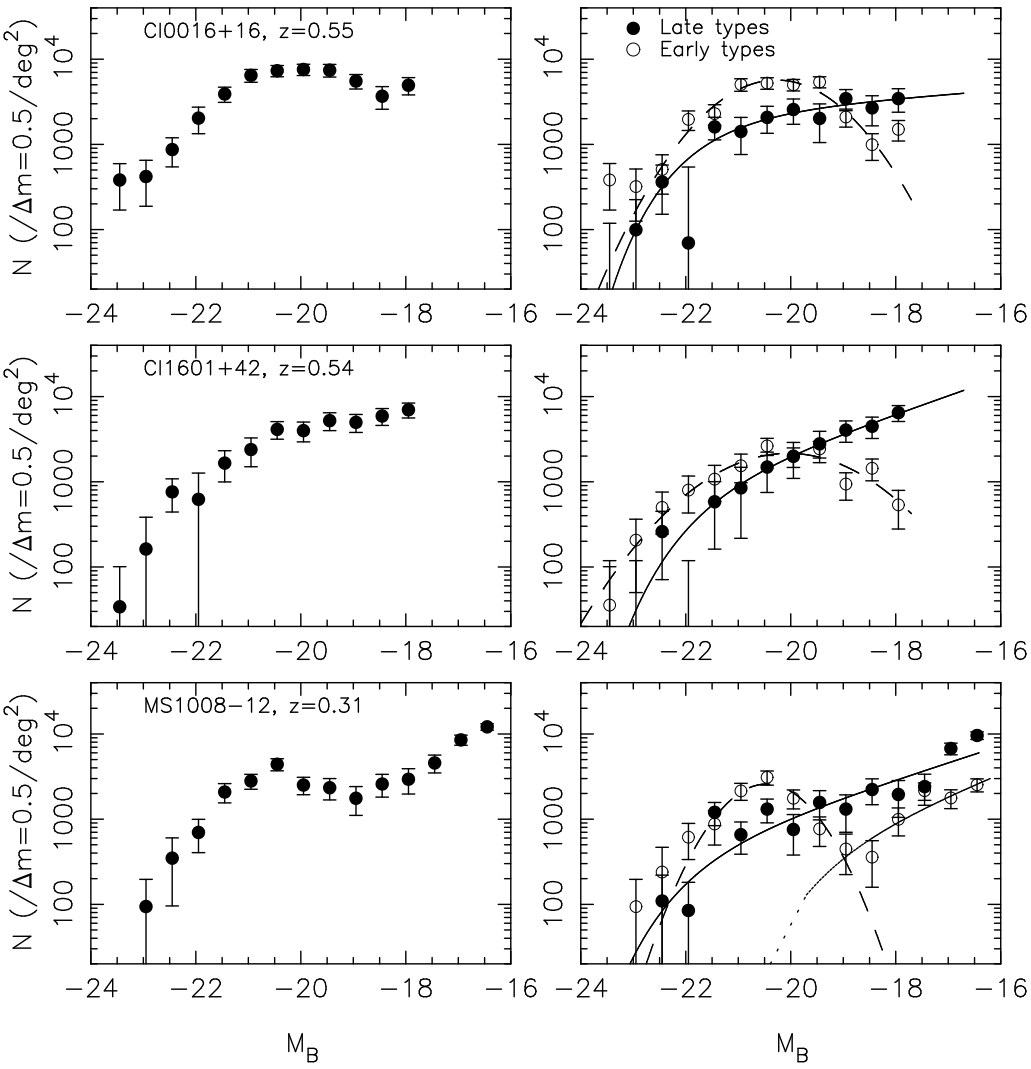

Figure 4: Luminosity functions in the rest-frame B–band for Cl0016+16, Cl1601+42 and MS1008-1224. The left panels show the total LFs, while in the right panels the LFs are divided into early-type (open circles) and late-type (filled circles) galaxies. Error-bars include Poissonian uncertainties and field-to-field variance. For MS1008-1224 we show separate Schechter fits for the early-type and late-type populations.

Table 8: The blue fraction, f_B, as defined by BO84, the absolute B magnitudes and rest-frame $B-V$ colour for the brightest cluster galaxy in our cluster sample and the early-type fraction at two limiting magnitudes.

Cluster	z	f_B	M_B	$B-V$	Early-type fraction	
					$M_B < -19.7$	$M_B < -17.7$
Cl0016+16	0.546	0.04 $\pm$ 0.02	-23.52 $\pm$0.02	1.00 $\pm$0.03	0.74$\pm$0.03	0.59$\pm$0.03
Cl1600+41	0.540	-	-23.36 $\pm$0.03	0.92 $\pm$0.05	0.55$\pm$0.15	0.31$\pm$0.07
Cl1601+42	0.539	0.15 $\pm$ 0.06	-23.50 $\pm$0.04	0.93 $\pm$0.07	0.63$\pm$0.04	0.36$\pm$0.03
MS1008-1224	0.306	0.13 $\pm$ 0.06	-23.65 $\pm$0.05	1.15 $\pm$0.07	0.59$\pm$0.03	0.36$\pm$0.02

4.3 The Butcher–Oemler effect

We calculate the blue fraction, f_B, with the conventional radius and limiting magnitude defined by BO84. In order to compare results we adopt the cosmology used by BO84 ($q_0 = 0.1$). The difference from BO84 is that we here select cluster members with the photometric redshift method. This increases the accuracy since background subtraction is reduced. The blue fractions derived are given in Table 8.

All values of f_B are located below the straight line fit of the blue fraction as a function of redshift presented in BO84. The scatter in this fit is, however, large, and at least for Cl1601+42 and MS1008-1224 this deviation is hardly significant. Cl0016+16 is included in the BO84 sample, and they also note that this cluster is exceptional in the sense that it has a fraction of blue galaxies that is more similar to local clusters than to clusters at $z > 0.3$. The blue fraction found by BO84 is $f_B = 0.02 \pm 0.07$, which is consistent with our estimate.

4.4 Brightest cluster galaxies

In Table 8 we list the absolute B magnitude and rest-frame $B-V$ colour for the brightest cluster galaxy (BCG) in the observed clusters, including the poor cluster Cl1600+41. Even though our sample is small, the results are consistent with the magnitude of the BCG being independent of the richness of the cluster, as shown by e.g. Sandage (1976) and Postman & Lauer (1995). In particular, we note that the BCG of the extremely poor cluster Cl1600+41 is only marginally fainter than the rest, demonstrating that even in this environment a luminous elliptical can be formed.

5 Discussion

5.1 Variations in the cluster luminosity function

The different shapes of the LFs in our sample show that there is no universal form of the total cluster LF at $z \gtrsim 0.3$ (Figure 4). We also find that a single Schechter function gives a poor representation of the cluster LF, which agrees with e.g. Driver et al. (1994) and Wilson et al. (1997). This is especially evident for MS1008-1224, where the best Schechter fit to $M_B < -17.7$ yields a faint-end slope that is decreasing, while the data-points clearly show an increase in the number of faint galaxies with $M_B > -19$.

From the separate late-type and early-type LFs (right panels of Figure 4), it is clear that the relative abundance of the early-type and the late-type populations determines the over-all shape of the LF.

In Cl1601+42 late-type galaxies dominate at $M_B \gtrsim -20$. This results in a total LF that increases over the whole magnitude range and has a steep faint-end slope. MS1008-1224 is similar to Cl1601+42 in that it contains a numerous population of faint late-type galaxies, which dominates the total LF at faint magnitudes. The magnitude where this cross-over takes place is, however, slightly fainter in MS1008-1224 ($M_B \sim -19.5$) compared to Cl1601+42 ($M_B \sim -20$), which

leads to a total LF where both an intermediate magnitude Gaussian part, as well as a steep faint-end slope of late-type galaxies are distinguishable. Note also that MS1008-1224 has a population of faint *early-type* galaxies, which adds to this.

In Cl0016+16 there are relatively few faint late-type galaxies, compared to the number of early-type galaxies at $-21 \lesssim M_B \lesssim -19$. This leads to a total LF that has a Gaussian shape at intermediate magnitudes, and only at the faintest bin is there an indication of a rise.

As discussed in DFN02, the differences between the shapes of the cluster LFs can be explained by the fact that clusters in the hierarchical clustering scenario at high redshift have a larger fraction of newly accreted galaxies with ongoing star formation. A general increase in the star formation rate in field galaxies with redshift (Diaferio et al. 2001), also contributes to an increase of star forming galaxies in clusters at high z.

After accretion, and a possible period of enhanced star formation, the galaxies could have their gaseous envelopes removed by tides or ram pressure stripping, leading to a fading over time-scales of Gyrs, as the remaining gas reservoir is exhausted (Balogh et al. 2000; Diaferio et al. 2001). Such a fading of the faint blue galaxies is discussed by Wilson et al. (1997), who argue that dwarf irregulars in clusters should fade by $\sim$ 3 mag since $z \sim 0.2$. Further, Conselice et al. (2001) show that spirals accreted at high z can be transformed into the faint dE population seen in local clusters by "galaxy harassment" (Moore et al. 1998).

It is of obvious interest to compare the LFs of the different populations of these clusters with those of nearby clusters like Coma and Virgo. We then have the paradoxical situation that studies of nearby cluster are limited to one, two or at most three colours, or alternatively to a morphological separation of different classes. A direct comparison with our spectral classification is therefore difficult. As a first step we therefore compare the *total* LF of our clusters with that of Coma at $z = 0.02$ (Trentham 1998a) and Virgo $z = 0.003$ (Trentham & Hodgkin 2002).

In Figure 5 we plot the rest-frame B–band LF for Cl1601+42 (open circles), Cl0016+16 (filled circles), and MS1008-1224 (triangles) together with the LF for the rich Coma cluster (squares) and the poor Virgo cluster (diamonds). For clarity, the LFs have arbitrary off-sets in the y-direction. As suggested by our discussion of the individual LFs, we represent the total LF as a sum of a Gaussian and a Schechter function.

5.1.1 The bright population

For Coma the Gaussian peaks at $M_B^G = -19.3 \pm 0.1$, indicating a fading of the bright population by $\Delta M \sim 1$ mag compared to the high redshift clusters (Table 7). The total LF of the Virgo cluster only has a marginal Gaussian peak. However, the population of morphologically classified early-type galaxies, as well as giant spirals, has a clear Gaussian shape peaking at $M_B^G \sim -19$ (Binggeli et al. 1988; Ferguson & Sandage 1991), supporting a fading of this population similar to that suggested for Coma.

These results are consistent with Smail et al. (1997), who find that the characteristic magnitude M_V^* for early-type galaxies fade by $\Delta M \sim 0.7$ mag between $z = 0.54$ and $z = 0$, where we have converted the results in Smail et al. to our adopted cosmology. Smail et al. find a weaker trend for bright spiral galaxies, which fade by $\Delta M \lesssim 0.4$ mag. An evolution is also found by Kodama & Bower (2001), who estimate that the bright blue galaxy population fades by $\Delta M \sim 1$ mag between $z \sim 0.4$ and $z = 0$.

5.1.2 The faint population

In DFN02 we argued that the different shapes of the LF at $M_B \gtrsim -20$ between Coma and Cl1601+42 can be understood as a result of the dynamically younger age of the latter cluster. The steep blue end of the LF in this cluster should then consist of recently accreted field galaxies, which is supported by the fact that this part of the LF is almost exclusively made up of late type galaxies. The rapidly increasing fraction of late-type galaxies in the outer parts of the cluster is consistent with this accretion scenario, and is reflected in the rising blue fraction at large radii in

this cluster, as shown in Section 5.3. A fading of the blue star forming galaxies in Cl1601+42 by $\sim$ 2 mag, would transform the LF of Cl1601+42 into a LF similar to Coma.

The steepening of the faint-end in MS1008-1224 is clearly shown in Figure 5. The slope is somewhat steeper compared to Coma, and is shifted towards brighter magnitudes. From Figure 4 we see that the faint-end of MS1008-1224 is made up of both blue and red galaxies. The slope of the faint blue population is similar to the blue population in Cl1601+42, and a fading by $\sim$ 1 mag of this population would result in a LF similar to the one in MS1008-1224. A subsequent fading by an additional magnitude will make both Cl1601+42 and MS1008-1224 similar to Coma. The fading of the late-type population between $z = 0.5$ and $z = 0$ for these two clusters could therefore be described by a relation $\Delta m \simeq -4z$ mag.

5.1.3 The red cluster Cl0016+16

The LF of Cl0016+16 at $z = 0.55$ differs clearly from Cl1601+42 at the same redshift. The LF of the former is similar to Coma in the plateau region, having a Gaussian shape, which is shifted to brighter magnitudes by $\sim$ 1 mag. From Figure 4 we see that the relatively low abundance of late-type galaxies in Cl0016+16, as compared to Cl1601+42, is responsible for the different shapes of the LF at intermediate magnitudes.

Previous investigations of Cl0016+16 also show that the bright galaxy population is dominated by red early-type galaxies. Koo (1981) found that this cluster has an unusually high fraction of red galaxies compared to other high redshift clusters, and suggested that the star formation must have ended a few Gyrs before the observed epoch. From the absence of blue galaxies and the small scatter in the colours of the red population Smail et al. (1995) conclude that the cluster is old, despite its high redshift. Of the ten clusters in the MORPHS sample (Smail et al. 1997) with morphological classification from HST in the redshift range $0.37 < z < 0.56$, Cl0016+16 has the lowest fraction of spiral galaxies, $f_{sp} = 21$ per cent, compared to a mean of $f_{sp} = 44 \pm 7$ per cent for the remaining nine clusters.

This is, not unexpectedly, related to the low blue fraction found in Cl0016+16, which indicates that the cluster does not follow the general blueing described by the BO-effect. A higher dynamical age for Cl0016+16 is supported by the high X-ray luminosity and velocity dispersion (Table 3), indicating that Cl0016+16 is more relaxed than Cl1601+42.

Cl0016+16 has a very high fraction of poststarburst galaxies. These galaxies have no current star formation, but were forming stars at $\sim$1–2 Gyr before we observe them. Poggianti et al. (1999) found that 32$\pm$9 per cent of the galaxies in Cl0016+16 are spectroscopically consistent with poststarburst galaxies. This suggests that a large fraction of the galaxies in Cl0016+16 has experienced star formation since $z \sim 0.8$, but has subsequently faded to become red at $z = 0.54$. Poststarburst galaxies are less frequent in local clusters (Poggianti et al. 1999), Cl0016+16 is therefore not similar to a local cluster placed at high redshift. This is also supported by the brighter early-type population in this cluster compared to local clusters.

The difference between rich clusters at high and low redshift can qualitatively be explained within the hierarchical clustering scenario. Kauffmann (1995) shows that rich clusters at high-z assemble over a shorter time interval than low-z clusters of similar richness. In general, this naturally leads to a higher fraction of blue galaxies in high-z clusters.

The properties of Cl0016+16 can be understood if it formed during a short time interval at $z \gtrsim 0.8$, leaving a high fraction of poststarburst galaxies. This suggests that the cluster was blue at $z \sim 0.8$, while the red colours at $z = 0.55$ indicates a very low infall of field galaxies during the last $\sim$ 1 Gyr before it is observed.

It is possible that the special environment of Cl0016+16 could have an influence on the blue fraction and the cluster LF. Connolly et al. (1996) and Hughes & Birkinshaw (1998) provide strong evidence that Cl0016+16 is part of a supercluster structure, with two associated clusters at similar redshift with projected distances of 5 and 13 Mpc. The formation of this giant structure could have depleted the number of field galaxies surrounding Cl0016+16, and therefore the accretion rate of late type galaxies.

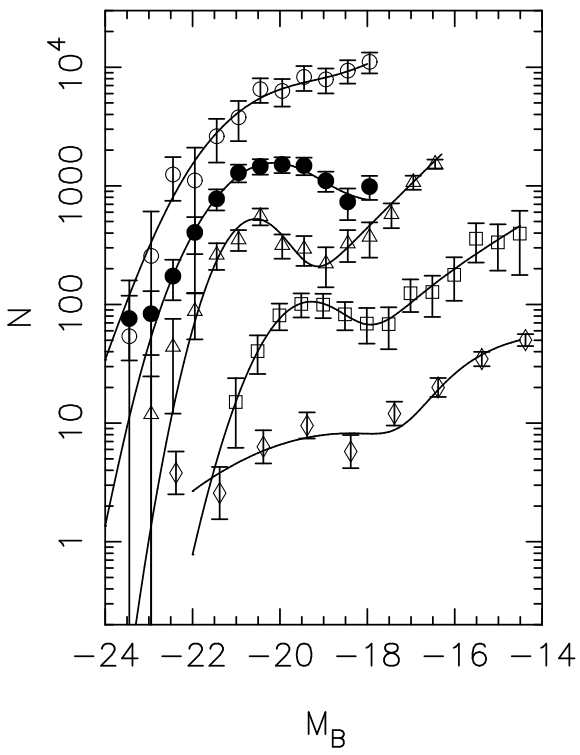

Figure 5: Luminosity function in the rest-frame B–band for Cl1601+42 at $z = 0.54$ (open circles), Cl0016+16 at $z = 0.55$ (filled circles), MS1008-1224 at $z = 0.31$ (triangles), Coma at $z = 0.02$ (squares) and Virgo at $z = 0.003$ (diamonds). Data for Coma and Virgo are taken from Trentham (1998a) and Trentham & Hodgkin (2002), respectively. The LFs are arbitrary off-set in the y-direction.

To summarise our discussion, we find no evidence for a universal shape of the total cluster LF, in agreement with e.g., Binggeli et al. (1988) and Driver, Couch & Phillipps (1998). The LFs for early-type and late-type galaxies separately has, however, similar shape in the different clusters, but with varying relative abundances. This supports the claim of universality of type-specific LFs (Binggeli et al. 1988; Andreon 1998), even though the parameters of the functions describing the type-specific LFs. e.g., the Gaussian width σ^G, varies between clusters. We argue that the different shapes of the high-z cluster LFs reflect different dynamical states of the clusters. As the clusters get dynamically older, we expect the late-type population to fade relative to the early-type population and LFs to become more similar.

5.2 The dwarf population in MS1008-1224

The faint limit in absolute magnitude we reach for MS1008-1224 at $z = 0.31$ allow us to study the dwarf population ~ 1.5 mag deeper in this cluster compared to the clusters at $z \sim 0.55$. To compare the colours of the dwarf population in MS1008-1224 with other nearby clusters, with more limited colour information, we plot in Figure 6 the rest-frame $B-R$ colours of galaxies with $-17.7 < M_B < -16.2$. Studies by Trentham (1998c) and Boyce et al. (2001) have shown that dIrr galaxies have $B-R \sim 0.9$, while dEs have colours in a broader range $1.3 \lesssim B-R \lesssim 2.0$.

In the $B-V$ histogram of MS1008-1224 in Figure 6 there are two peaks, suggesting that there indeed are two distinct populations representing dIrrs and dEs. In the figure we also show the distribution of $B-R$ colours for the faint galaxies, which on the basis of the full $BVRI$ photometry we have classified as early-type and late-type galaxies. The fact that this classification closely follows the two colour division into the two peaks shows that we reliably can use the $B-R$ colour

to distinguish between early-type and late-type galaxies.

From the $B-R$ colours Trentham (1998c) finds that all dwarf galaxies with $-18.9 < M_R < -16.9$ in Abell 665 at $z = 0.18$ are consistent with being dEs (called dSphs by Trentham). In Abell 963 at $z = 0.21$ the majority of the dwarf galaxies with $-19.2 < M_R < -18.2$ also have colours consistent with dEs. There is, however, in this cluster also a population with colours intermediate between dEs and dIrrs, which Trentham proposes may represent a transitional stage between these types.

In a recent study Boyce et al. (2001) investigate the $B-R$ colour of galaxies with $-19 < M_R < -16.5$ in the cluster Abell 868 at $z = 0.154$. They find a distribution in colour with two peaks, showing the presence of a dominant population of dEs, but also a population of dIrrs. For the faintest galaxies ($-17.5 < M_R < -16.5$) there are similar numbers of dEs and dIrrs.

The main difference between MS1008-1224 and lower redshift clusters is the relative fraction of dIrrs to dEs. To make a quantitative comparison between the faint populations, we use the $B-R$ index to calculate the fraction of dIrrs for MS1008-1224, Abell 963, Abell 665 and Abell 868. We assume that galaxies with rest-frame $B-R < 1.2$ are dIrrs, which is the criterion used by Boyce et al. (2001).

A complication is that MS1008-1224 is not observed in standard Johnson-Cousins filters, but in Bessel filters. To correct for this we use galaxy templates from Coleman et al. (1980) and filter transmission curves to calculate the transformation between the standard $B-R$ colours and the $B-R$ colours for the Bessel filters. We find that the division between dIrrs and dEs at $B-R = 1.2$ in standard Johnson-Cousins filters corresponds to $B-R = 1.34$ in the Bessel filters.

Using this criterion, we find that the fraction of faint galaxies that belong to the dIrr population is 0.72 ± 0.03 for MS1008-1224, to be compared with 0.07 ± 0.03 for Abell 963, 0.01 ± 0.01 for Abell 665 and 0.22 ± 0.02 for Abell 868. A further problem when comparing these numbers is that the different investigations use different magnitude intervals for defining the dwarf populations. Irrespective of this, however, we reach the important conclusion that MS1008-1224 is dominated by dIrrs, while the other clusters are dominated by dEs.

The fraction of dIrrs in Coma, classified by the same colour criterion as above, for galaxies with $-15.3 < M_R < -13.3$ is 0.11 ± 0.01 (calculated from Figure 7 in Trentham 1998a). The fraction of *morphological* dIrrs in Virgo ($-17.8 < M_B < -15.8$) is 0.25 ± 0.07 (calculated from Figure 6 in Trentham & Hodgkin 2002). The results emphasise the conclusion that dEs dominate the faint population in nearby clusters, while our study shows that the opposite is true for MS1008-1224 at $z = 0.31$. It would obviously be of great interest to study more clusters to these limits to see if this is a general property.

Galaxy harassment could here be a mechanism that transforms the faint late-type population, dominating medium redshift clusters such as MS1008-1224, into dEs, as shown by Conselice et al. (2001). The similarity between the faint-end slopes of the late-type population ($\alpha_f = -1.84 \pm 0.12$) and the early-type population ($\alpha_f = -1.69 \pm 0.14$) at faint magnitudes ($M_B > -19$) is naively consistent with this picture.

5.3 Galaxy populations as a function of radius

Ellingson et al. (2001) show that late-type galaxies start to dominate closer to the cluster core in high redshift clusters. This is explained as a consequence of the higher infall rate at high redshift, which leads to a higher fraction of late-type galaxies at radii just outside the central core in high-z clusters.

In Figure 7 we plot as solid lines the morphological gradients by Ellingson et al., where morphological early-type fractions are taken from Whitmore, Gilmore & Jones (1993)($z = 0$) and Dressler et al. (1997)($z = 0.4$). Here we have converted the radius given in units r_{200}, which is the radius within which the average cluster density is 200 times the cosmic critical density, by setting $r_{200} \sim 1\ h^{-1}$ Mpc, which is the same assumption as used by Ellingson et al. In the Figure we plot the radial dependence of the early-type fractions of the clusters in our sample, using the same limiting magnitude as Dressler et al. We find that Cl1601+42 and MS1008-1224 have radial gradients significantly steeper than local clusters, which therefore support the results of Ellingson

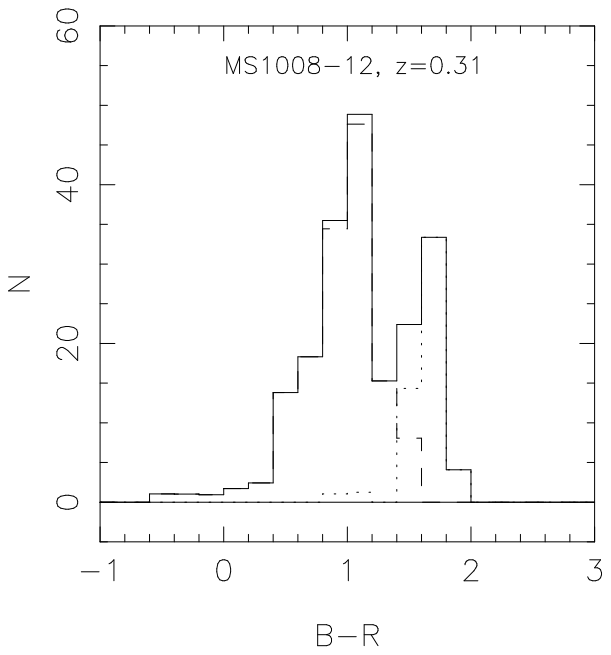

Figure 6: The rest-frame $B - R$ colour distribution for galaxies in MS1008-1224 with $-17.7 < M_B < -16.2$. The solid line shows the total number of galaxies, while the dotted and dashed lines show the distribution of early-type and late-type populations, as classified by multi-band photometry, separately.

et al. The atypical cluster Cl0016+16 has a population gradient similar to low redshift clusters, consistent with a low recent infall rate onto this cluster.

van Dokkum et al. (2000, 2001) show that the morphologic early-type fraction in rich clusters decreases from $\sim$ 0.8 at $z = 0$ to $\sim$ 0.5 at $z \sim 1$. If we compare the photometric early-type fractions of bright cluster galaxies ($M_B < -19.7$) given in Table 8 with this trend, we find that three of our clusters has a fraction $\sim$ 0.6, which is lower than the local value and consistent with van Dokkum et al., while Cl0016+16 has an early-type fraction $\sim$ 0.74, which is significantly above the other, and similar to local clusters.

However, there is not a one-to-one correspondence between our photometric classification and the morphological classification used by van Dokkum et al. and Ellingson et al. To see how well these classifications match, we use a sample of 195 cluster galaxies in Cl0016+16 and Cl1601+42 with determined photometric types, as well as morphologies determined from HST observations (Smail et al. 1997). We find that 72 per cent of the galaxies are photometric early-types, while 66 per cent are morphological E0-Sa galaxies and 59 per cent are are morphological E0-S0 galaxies.

This shows that the early-type fraction determined from photometry is somewhat higher than the fraction determined from morphology. This is especially evident if E0 and S0 galaxies, but not Sa galaxies, are regarded as morphologic early-types. The reason for the lack of a one-to-one correspondence between the classifications is the existence of a population of photometrically red Sb, or later type galaxies. There are also E0-S0 galaxies with blue colours that are photometrically classified as late-types.

The clusters in Table 8 with a photometric early-type fractions $\sim$ 0.6 should therefore have morphological early-type fractions somewhat below this, which is consistent with the decreasing morphological early-type fraction with redshift found by van Dokkum et al. Even if the morphological early-type fraction in Cl0016+16 is lower than the photometric, this cluster should still have a high fraction, well above the other clusters at similar redshift.

Previous studies have shown that the ratio of faint to bright galaxies increases at large radii, where the surface density decreases. Driver et al. (1998) find that five of seven clusters at $z \sim 0.15$

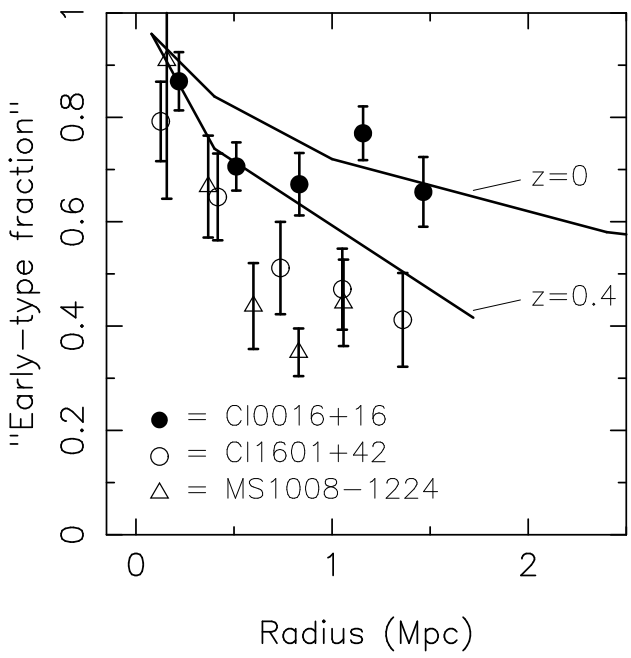

Figure 7: Early-type fractions for Cl0016+16, Cl1601+42 and MS1008-1224. Shown are also the morphological gradients presented by Ellingson et al. (2001), where morphological early-type fractions are taken from Whitmore et al. (1993)($z = 0$) and Dressler et al. (1997)($z = 0.4$).

show an increasing dwarf-to-giant ratio with radius. A K-band study of AC 118 at $z = 0.3$ by Andreon (2001) shows the same trend. In DFN02 we found that Cl1601+42 has a steeper faint-end slope of the LF in the outer part of the cluster, which is equivalent to an increasing dwarf-to-giant ratio.

Here, we calculate the dwarf-to-giant ratio by defining galaxies with $-19.5 < M_B < -17.7$ as dwarfs, and brighter galaxies as giants. The separation between dwarfs and giants is chosen to match the cross-over in the cluster LFs between early-type and late-type galaxies (Figure 4). This division is somewhat brighter than used in other papers (e.g., Driver et al. 1998), and is here adopted in order to get sufficient statistics in the faint bin. We further divide each cluster into a core region with projected radius < 0.5 Mpc, and an outer region between 0.5 and 1.1–1.5 Mpc, depending on cluster.

In Figure 8 we plot the resulting dwarf-to-giant ratios as function of surface density of the giant galaxies for these two regions in all clusters. Cl0016+16 is represented by circles, Cl1601+42 by squares and MS1008-1224 by triangles. Filled symbols show results for the core area, while open symbols represent results from the outer area. The horizontal lines represent the field value and the corresponding 1σ-errors.

Figure 8 shows that Cl0016+16 and Cl1601+42 have a clear trend of an increasing dwarf-to-giant ratio when going from the inner high density region, to the outer lower density region, which is consistent with the trend found by Phillipps et al. (1998) and with Andreon (2001). As an explanation of this these authors suggest that the high density environment in cores of clusters is hostile to the dwarf galaxies, while the outer, low density regions do not affect this population, which therefore have a dwarf-to-giant ratio and faint-end slope similar to that of the field.

For the low redshift cluster MS1008-1224, we do not see any trend. We note, however, that the error in the dwarf-to-giant ratio is substantial.

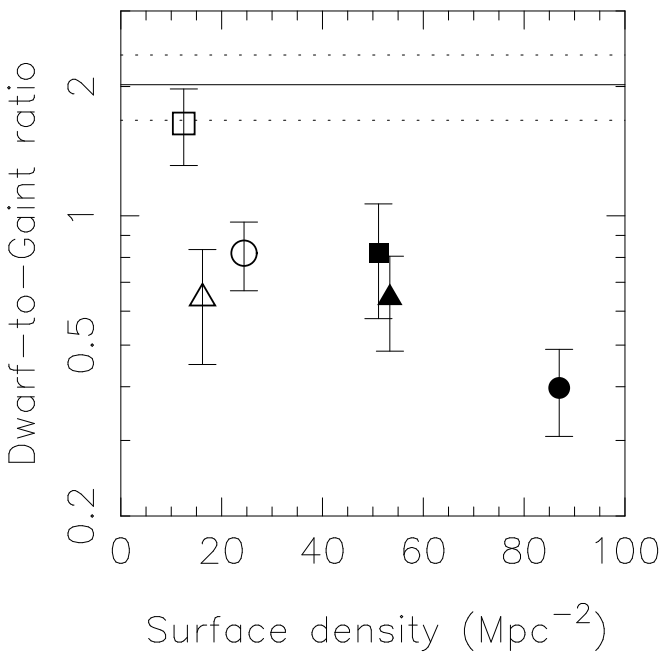

Figure 8: Dwarf-to-giant ratio as a function of bright galaxy surface density for Cl0016+16 (circles), Cl1601+42 (squares) and MS1008-1224 (triangles). Filled symbols represent the inner region of the cluster ($R < 0.5$ Mpc), while open symbols represent the outer region. The horizontal lines represent the field value (solid line) and 1σ-errors (dotted lines).

5.4 The Butcher–Oemler effect as function of radius and limiting magnitude

The BO effect is of major observational importance as a probe of the galaxy population. Although much of the discussion below to a large extent is a consequence of the early-type and late-type LFs in Figure 4 and their dependence on radius (e.g., Figure 3), we will for this reason illustrate this with two important implications for the BO effect.

Already in BO84 and more recently in DFN02 it is pointed out that the blue fraction f_B increases at larger radii. This can be understood as a result of the fact that ellipticals are in general more centrally concentrated than spirals. In Figure 9 we show the dependence of f_B on radius, where the radius is given in fractions of R_{30}, which is the nominal radius given by BO84, and is defined as the radius inside of which 30 per cent of the cluster galaxies with $M_V < -20$ are contained.

Also in this respect Cl0016+16 deviates from the other clusters. Inside of $1.25R_{30}$, f_B decreases rapidly, while outside this radius f_B stays almost constant, at a value well below that of the other clusters. Cl1601+42 on the other hand shows a steep radial dependence. The higher blue fraction in Cl1601+42 is consistent with the higher fraction of late type galaxies in this cluster (Figure 3). MS1008-1224 has a trend in between the two higher redshift clusters. From a very low f_B in the core region, there is a rapid increase to $\sim$ 1.25 R_{30}, followed by a slower increase in the outer regions. The behaviour of f_B in these clusters reflects, as expected, the radial dependence of the early-type fraction shown in the right panel of Figure 3.

In DFN02 we showed that f_B in Cl1601+42 depends strongly of the limiting magnitude. This dependence is a direct consequence of the different shapes of the early-type and late-type LFs in this cluster. At fainter magnitudes the total LF becomes more dominated by late-type galaxies, which leads to a higher f_B. In Figure 10 we plot the dependence of f_B on the limiting magnitude for the three clusters. As expected, the increase of f_B is much weaker in Cl0016+16 than in Cl1601+42, which is consistent with the LF for this cluster being dominated by early-type galaxies to fainter

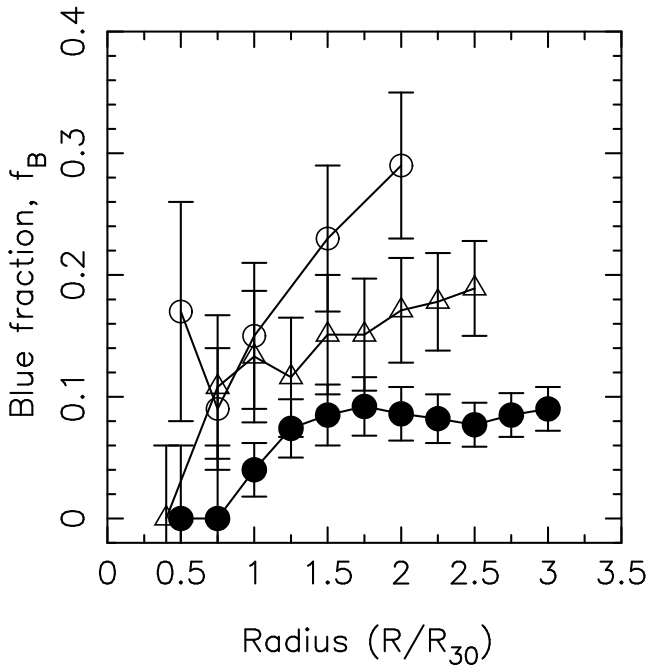

Figure 9: The blue fraction, f_B, as a function of radius for Cl0016+16 (filled circles), Cl1601+42 (open circles) and MS1008-1224 (triangles). R_{30} is the fiducial value used by BO84 for calculating f_B.

magnitudes (Figure 4). MS1008-1224 again shows an intermediate behaviour. The strong increase in f_B at faint magnitudes in MS1008-1224 is caused by the dominating population of blue dwarf galaxies.

6 Summary

This work represents one of the deepest studies of the LF for intermediate redshift clusters, several magnitudes beyond L^*. This has been possible, despite the moderate telescope size, by using photometric redshifts. Our main conclusions are:

- There is no universal shape of the total cluster LF at $z \gtrsim 0.3$.
- The early-type population has a Gaussian shaped LF, while the late-type population is well fitted by a Schechter function. This suggests that the LFs for different populations could be universal, while the total LF depends on the relative abundance of these populations.
- The evolution of the late-type galaxies is consistent with a fading by ~ 2 magnitudes between $z \sim 0.55$ and $z = 0$, while the early-type population fades by ~ 1 mag. This scenario suggests that the total LFs of the high-z clusters become more similar to local LFs as the clusters get dynamically older.
- The red cluster Cl0016+16 is an atypical high-z cluster that resembles local rich clusters in many aspects, indicating an old dynamical age despite its redshift. It does, however, contain a large fraction of poststarburst galaxies, suggesting that the cluster was bluer at $z \gtrsim 0.8$, and that the infall was very low during ~ 1 Gyr before the cluster is observed.
- In MS1008-1224 at $z = 0.31$, we find that dIrrs dominate over dEs, opposite to what is found in nearby clusters.

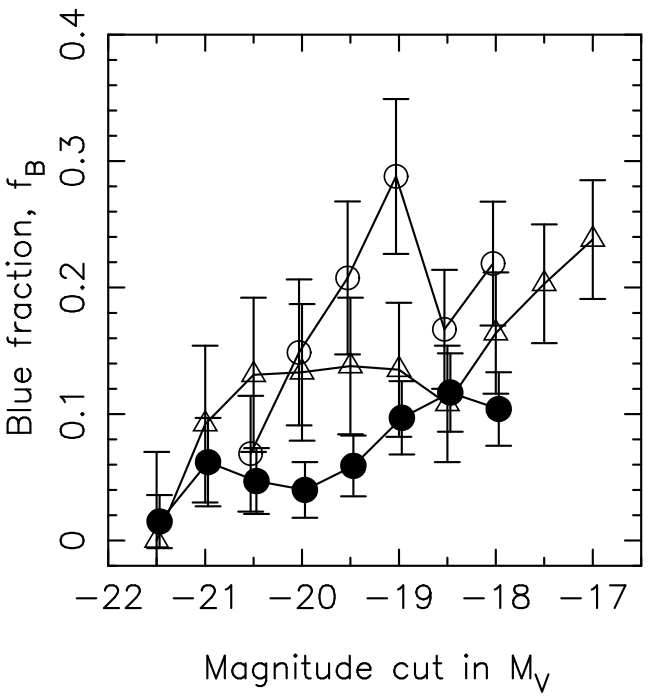

Figure 10: The fraction of blue galaxies, f_B, as a function of limiting magnitude for Cl0016+16 (filled circles), Cl1601+42 (open circles) and MS1008-1224 (triangles).

- The relation between dwarf-to-giant ratio and surface density indicates that high density regions are hostile to dwarfs, consistent with a destruction or fading of this population by galaxy harassment.
- We find that the blue fraction, f_B, as defined by BO84 varies with radius and limiting magnitude. This is a direct consequence of the radial gradient of the late-type galaxies and the relative normalisation of the late-type and early-type LFs.

Acknowledgements

Nordic Optical Telescope is operated on the island of La Palma jointly by Denmark, Finland, Iceland, Norway, and Sweden, in the Spanish Observatorio del Roque de los Muchachos of the Instituto de Astrofisica de Canarias.

The data presented here have been taken using ALFOSC, which is owned by the Instituto de Astrofisica de Andalucia (IAA) and operated at the Nordic Optical Telescope under agreement between IAA and the NBIfAFG of the Astronomical Observatory of Copenhagen.

This paper is also based on observations obtained at the Very Large Telescope at Cerro Paranal operated by the European Southern Observatory.

This work has been supported by the Swedish Research Council.

References

Andreon S., 1998, A&A, 336, 98

Andreon S., 2001, ApJ, 547, 623

Balogh M.L., Navarro J.F., Morris S.L. 2000, ApJ, 540, 113

Baugh C.M., Cole S., Frenk C.S. 1996, MNRAS, 282, L27

Benitez N., 2000, ApJ, 536, 571

Binggeli B., Sandage A., Tammann G.A., 1988, ARA&A, 26, 509

Bower R.G., 1991, MNRAS, 248, 332

Bower R.G., Kodama T., Terlevich, A., 1998, MNRAS, 299, 1193

Boyce P.J., Phillipps S., Jones J.B., Driver S.P., Smith R.M., Couch W.J. 2001, MNRAS, 328, 277

Brunner R.J., Lubin L.M., 2000, AJ, 120, 2851

Butcher H., Oemler A., 1984, ApJ, 285, 426 (BO84)

Carlberg R.G., Yee H.K.C., Ellingson E., Abraham R., Gravel P., Morris S., Pritchet C.J. 1996, ApJ, 462, 32

Coleman G.D., Wu C.–C., Weedman D.W., 1980, ApJS, 43, 393

Connolly A.J., Szalay A.S., Koo D., Romer A.K., Holden B., Nichol R.C., Miyaji T., 1996, ApJ, 473, 67

Conselice C.J., Gallagher J.S., Wyse R.F.G., 2001, ApJ, 559, 791

da Costa, L.N., et al., 1998, submitted to A&A, (astro-ph/9812105), under revision and update

Dahlén T., Fransson C., Näslund M. 2002, MNRAS, 330, 167 (DFN02)

Diaferio A., Kauffmann G., Balogh M.L., White S.D.M., Schade D., Ellingson E. 2001, MNRAS, 323, 999

Dressler A., Gunn J.E. 1992, ApJS, 78, 1

Dressler A., et al., 1997, ApJ, 490, 577

Dressler A., Smail I., Poggianti B.M., Butcher H., Couch W.J., Ellis R.S., Oemler A., 1999, ApJS, 122, 51

Driver S.P., Phillipps S., Davies J.I., Morgan I., Disney M.J., 1994, MNRAS, 268, 393

Driver S.P., Couch W.J., Phillipps S., 1998, MNRAS, 301, 369

Dubinski J., 1998, ApJ, 502, 141

Ellingson E., Lin H., Yee H.K.C., Carlberg R.G., 2001, ApJ, 547, 609

Ferguson H.C., Sandage A., 1991, AJ, 101, 765

Gioia I.M., Luppino G.A., 1994, ApJS, 94, 583

Gunn J.E., Stryker L.L., 1983, ApJS, 52, 121

Henry J.P., Soltan A., Briel U., Gunn J.E. 1982, ApJ, 262, 1

Hughes J.P., Birkinshaw M. 1998, ApJ, 497, 645

Jarvis J.F., Tyson J.A., 1981, AJ, 86, 476

Kauffmann G., 1995, MNRAS, 274, 153

Kauffmann G., White S.D.M., Guiderdoni B., 1993, MNRAS, 264, 201

Kodama T., Bell E.F., Bower R.G., 1999, MNRAS, 302, 152

Kodama T., Bower R.G., 2001, MNRAS, 321, 18

Koo D.C., 1981, ApJ, 251, L75

Landolt A.U., 1992, AJ, 104, 340

Lewis A.D., Ellingson E., Morris S.L., Carlberg R.G., 1999, ApJ, 517, 587

Liu C.T., Green R.F., 1998, AJ, 116, 1074

Madau P., 1995, ApJ, 441, 18

Margoniner V.E., de Carvalho R.R., Gal R.R., Djorgovski S.G., 2001, ApJ, 548, 143

Moore B., Lake G., Katz N., 1998, ApJ, 495, 139

Näslund M., Fransson C., Huldtgren M. 2000, A&A, 356, 435

Oke J.B., Gunn J.E., Hoessel J.G., 1996, AJ, 111, 29

Phillipps S., Driver S.P., Couch W.J., Smith R.M., 1998, ApJ, 498, L119

Poggianti B.M., Smail I., Dressler A., Couch W.J., Berger A.J., Butcher H., Ellis R.S., Oemler A., 1999, ApJ, 518, 576

Postman M., Lauer T.R. 1995, ApJ, 440, 28

Rakos K.D., Schombert J.M., 1995, ApJ, 439, 47

Sandage A., 1976, ApJ, 205, 6

Schlegel D.J., Finkbeiner D.P., Davis M. 1998, ApJ, 500, 525

Schechter P., 1976, ApJ, 203, 297

Smail I., Ellis R.S., Fitchett M.J., Edge A.C., 1995, MNRAS, 273, 277

Smail I., Dressler A., Couch W.J., Ellis R.S., Oemler A., Butcher H., Sharples R.M., 1997, ApJS, 110, 213

Smail I., Edge A.C., Ellis R.S., Blandford R.D., 1998, MNRAS, 293, 124

Smith R.M., Driver S.P., Phillipps S., 1997, MNRAS, 287, 415

Trentham N., 1998a, MNRAS, 293, 71

Trentham N., 1998b, MNRAS, 294, 193

Trentham N., 1998c, MNRAS, 295, 360

Trentham N., Hodgkin S., 2002, MNRAS, in press

Valdes F., 1982, Faint Object Classification and Analysis System. NOAO, Tucson, AZ

Valdes F., 1993, FOCAS User's Guide. NOAO, Tucson, AZ

van Dokkum P.G., Franx M., Fabricant D., Kelson D.D., Illingworth G.D., 1999, ApJ, 520, L95

van Dokkum P.G., Franx M., Fabricant D., Illingworth G.D., Kelson D.D., 2000, ApJ, 541, 95

van Dokkum P.G., Stanford S.A., Holden B.P., Eisenhardt P.R., Dickinson M., Elston R., 2001, ApJ, 552, L101

Whitmore B.C., Gilmore D.M., Jones C., 1993, AJ, 407, 489

Wilson G., Smail I., Ellis R.S., Couch W.J., 1997, MNRAS, 284, 915

Yagi M., Kashikawa N., Sekiguchi M., Doi M., Yasuda N., Shimasaku K., Okamura S., 2002, AJ, 123, 87

Yee H.K.C., Ellingson E., Morris S.L., Abraham R.G., Carlberg R.G., 1998, ApJS, 116, 211